IEEE Access
Multidisciplinary | Rapid Review | Open Access Journal

Received October 22, 2020, accepted November 26, 2020, date of publication December 3, 2020,
date of current version December 15, 2020.

Digital Object Identifier 10.1109/ACCESS.2020.3042236

Broadband Vortex Beams Generation With Narrow Divergence Angle Using Polarization Insensitive Metasurface

HONGYU MA[1], XIANGLIN KONG[1,2], (Member, IEEE), PENG CHEN[1,2], (Member, IEEE), WEIHUA WANG[3], KUI HAN[3], LEI ZHAO[2], (Senior Member, IEEE), AND XIAOPENG SHEN[3], (Member, IEEE)

[1]National and Local Joint Engineering Laboratory of Internet Application Technology on Mine, China University of Mining and Technology, Xuzhou 221116, China
[2]School of Information and Control Engineering, China University of Mining and Technology, Xuzhou 221116, China
[3]School of Materials Science and Physics, China University of Mining and Technology, Xuzhou 221116, China

Corresponding authors: Xiaopeng Shen (xpshen@cumt.edu.cn) and Lei Zhao (leizhao@cumt.edu.cn)

This work was supported in part by the Six Talent Peaks Project in Jiangsu Province under Grant XYDXX-072, and in part by the National Natural Science Foundation of China under Grant 61372048 and 61771226, and in part by the Natural Science Foundation of Jiangsu Province under Grant BK20161186.

ABSTRACT In this paper, we propose a polarization insensitive metasurface to generate broadband vortex beams with narrow divergence angle. The metasurface is composed of 30 × 30 I-shaped metal elements printed on the F4B substrate with metal ground plane. The wideband is realized by optimizing the parameters of I-shaped unit cell to adjust the resonant frequency. A 360° phase range is achieved by rotating the element along the central axis. The phase superposition method is used to design the metasurface to generate vortex beams with narrow divergence angle. The proposed metasurface can generate broadband vortex beams under circular polarization (CP) and linear polarization (LP) wave excitation. The far-field radiation patterns and near-field characteristics of the metasurface are simulated to verify the proposed design. The gain of vortex beams is better than 15 dBi within 12-20 GHz (relative bandwidth of 50%), and the maximum gains are 23.2 dBi, 25.3 dBi for CP and LP cases, respectively. The broadband metasurface is fabricated and measured, and the measured results agreed well with the simulated ones. The proposed design provides a convenient and flexible way to realize broadband vortex beams with narrow divergence angle.

INDEX TERMS Metasurface, orbital angular momentum (OAM), vortex beam, polarization insensitive, narrow divergence angle.

I. INTRODUCTION

In recent decades, vortex beams have become a research hotspot owing to their spiral phase front carrying orbital angular momentum (OAM) [1]–[6]. The OAM waves have demonstrated to improve the spectrum efficiency and communication capacity by its theoretically infinite number of non-interfering orthogonal channel with different modes [7], [8]. Therefore, it is very critical to find an efficient method for realizing vortex beams. In 2007, Thide proposed the concept of electromagnetic (EM) vortex, and used an antenna array to generate vortex waves in the radio frequency domain [9]. After that, various ways have been proposed to produce vortex beams in the fields of radio frequency communication, such as spiral reflectors [10], antenna array [11]–[13], and circular traveling-wave antenna [14]. Although these conventional methods can generate vortex beams successfully, the performance of high gains and the simplicity of the design need to be further improved. In 2011, Yu *et al.* firstly proposed and used metasurface with V-shaped array to generate vortex beams [15], and Cui *et al.* proposed the concept of digital coding metasurface in 2014 [16], [17]. Both methods can be applied to generate vortex beams easily and efficiently.

Recently, metasurfaces have made remarkable progress in generating electromagnetic vortex beams [18]–[25]. In [26]–[29], single-layer or multi-layer metasurfaces are designed by varying the structural parameters of

The associate editor coordinating the review of this manuscript and approving it for publication was Luyu Zhao.

meta-atom patch to generate narrowband vortex waves. Besides, the broadband vortex waves were obtained by Pancharatnam-Berry (PB) metasurfaces in [30]–[33]. Although these designs can successfully realize perfect vortex beams, they are only suitable for LP or CP waves incidence. Xu and Liu *et al.* proposed a dual-layer metasurface using PB cells to generate vortex beams, which can be adapted for LP and CP waves [34]. Nevertheless, the above metasurface limits its application in vortex communication due to its multilayer design and large divergence angle. Therefore, it is highly demanded to seek a single-layer polarization insensitive metasurface to achieve broadband vortex beam with narrow divergence angle.

In this paper, a single-layer metasurface for generating wideband vortex beams is proposed by employing I-shaped unit cells. A complete 360° reflection phase range can be realized by rotating the meta-atom. The unit cells are arranged to build a metasurface according to the superposed phase distribution. Finally, a prototype is fabricated and measured. Both simulated and measured results confirm the feasibility of the design. The proposed vortex beam metasurface has the following advantages: 1) the design can realize wideband vortex beam from 12 GHz to 20 GHz (relative bandwidth of 50%), 2) the metasurface can generate narrow divergence angle vortex beam with high gain that is better than 15 dBi in the working band, 3) the design is applicable to both CP and LP wave excitations, which provides a flexible way to generate OAM beams.

II. BROADBAND META-ATOM DESIGN

For a reflective metal-atom under Cartesian coordinate system, as shown in Fig. 1, the reflection parameters with a rotation angle Φ under CP wave incidence can be expressed as follows:

$$r_{LL} = \frac{1}{2}[(r_{xx} - r_{yy}) - j(r_{xy} + r_{yx})]e^{-j2\Phi} \quad (1a)$$

$$r_{RR} = \frac{1}{2}[(r_{xx} - r_{yy}) + j(r_{xy} + r_{yx})]e^{j2\Phi} \quad (1b)$$

$$r_{LR} = \frac{1}{2}[(r_{xx} + r_{yy}) + j(r_{xy} - r_{yx})] \quad (1c)$$

$$r_{RL} = \frac{1}{2}[(r_{xx} + r_{yy}) - j(r_{xy} - r_{yx})] \quad (1d)$$

In equation (1), r_{LL}, r_{RR} are the co-polarized reflection coefficients and r_{LR}, r_{RL} are the cross-polarized reflection coefficients under normal CP wave incidence. Theoretically, when $|r_{xy}| \approx |r_{yx}| \approx 1$, and $r_{xx} \approx r_{yy} \approx 0$, no phase difference exists between the two cross-polarized reflection waves, which means that the 100% effective reflective PB phase can be obtained.

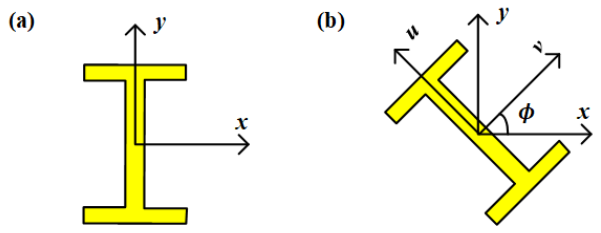

FIGURE 1. Reflective metal-atom in (a) xyz coordinates and (b) coordinates with a rotation angle Φ.

To broaden the working bandwidth, the phase response curves of the designed meta-atom should have similar slopes at different frequencies within a frequency range, and it can be written as:

$$\frac{\partial\varphi(L,L)}{\partial f_{min}} \approx \frac{\partial\varphi(L,L)}{\partial f_i} \approx \frac{\partial\varphi(L,L)}{\partial f_{max}} \quad (2)$$

Therein, f_{min} and f_{max} are the upper and lower limits of the working bandwidth respectively, and f_i is the value of arbitrary frequency within the broadband. The $\varphi(L, L)$ is the reflection phase under the normal incidence of the LCP wave, and the expression also satisfies the condition of the RCP wave incidence. In addition, the meta-atoms with different rotation angles need to have the same reflection amplitude.

Based on the above theory, a reflective meta-atom is designed to realize all the mathematical characteristics in a certain frequency bandwidth. The proposed unit cell is composed of I-shaped metal patch printed on the dielectric layer F4B ($\boldsymbol{\varepsilon_r} = 2.65$, $\tan\sigma = 0.001$) with the metal ground, as shown in Fig. 2(a). In addition, the structural parameters of each unit cell are as follows, $p_x = p_y = 8$ mm, $b = 4$ mm, $a = 3.2$ mm, $h = 3$ mm. The continuous phase distribution from 0° to 360° can be obtained by varying the angle between the element and the central axis.

The electromagnetic parameters of meta-atom are investigated in CST microwave studio, which are shown in Figs. 2(b)-2(f). In Fig. 2(b), the cross-polarized reflection coefficients are approximately equal to 1 ($|r_{xy}| \approx |r_{yx}| \approx 1$) and co-polarized reflective amplitudes are lower than 0.2 ($|r_{xx}| \approx |r_{yy}| < 0.2$) under x- or y-polarized waves incidence. Fig. 2(c) shows the co-polarized and cross-polarized reflection coefficients under normal incidence with left circular polarization (LCP) wave. The former coefficient is higher than 0.95 ($|r_{LL}| > 0.95$), and the latter coefficient is suppressed below 0.2 ($|r_{RL}| < 0.2$). Without considering the aperture efficiency, the working efficiency can be calculated as $\eta = 2\left|\left(|r_{xy}|+|r_{yx}|\right)/2\right|^2 / \left[|r_{xx}|^2+|r_{yy}|^2+|r_{xy}|^2+|r_{yx}|^2\right]$, which is higher than 95% from 11 GHz to 21 GHz. Fig. 2(d) shows the reflection amplitude and phase of I-shaped metal structures with different rotation angles. We can see that the phase shift of a reflective wave is twice the rotation angle. Figs. 2(e) and (f) show the reflection amplitude and phase under LCP wave incidence with different incident angle. In Fig. 2(e), the reflection amplitude is better than 0.95 under the incident angle increase from 0° to 40° within 12 GHz-20 GHz. In Fig. 2(f), the reflection phase change in a little range under incident angle within 0°-30°, and the phase sharply increases when the incidence angle is up to 40°. The stability of the incidence angle within 0°-30° fully meets our design requirement.

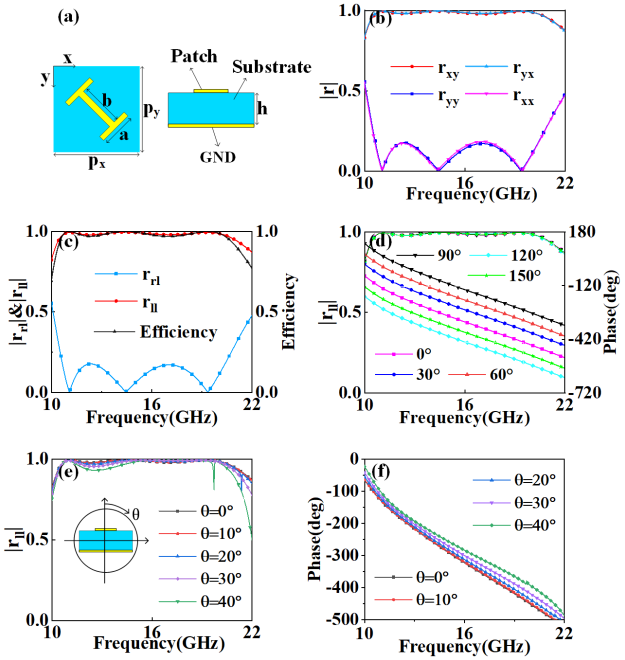

FIGURE 2. Numerically calculated EM response of the proposed element. (a) Topology of the unit cell. (b) Reflection coefficients under x- and y-polarized incidence. (c) Reflection coefficients under left circular polarization (LCP) excitation and the efficiency. (d) Reflection amplitude and phase for elements with different rotation angles under LCP incidence. (e) Normalized amplitude in different incident angle. (f) Phase in different incident angle.

III. VORTEX BEAMS METASURFACE DESIGN

In theory, the metasurface with vortex phase distribution can easily generate vortex beams under plane waves incidence. The vortex phase distribution can be written as:

$$\varphi_1(x, y) = l \tan\left(\frac{y}{x}\right) \tag{3}$$

where l is the OAM mode number of phase singularity, also called topological charge. The metasurface is designed in this paper to generate the vortex beam with $l = 1$.

The feed antenna radiates EM waves with spherical wavefront, which cannot meet the incidence condition of metasurface with the vortex phase distribution. Hence, it is necessary to combine the focusing phase distribution to convert spherical waves into spiral wavefront. The required focusing phase function can be expressed as:

$$\varphi_2(x, y) = \frac{2\pi}{\lambda}\left(\sqrt{F^2 + x^2 + y^2} - F\right) \tag{4}$$

where x, y are spatial coordinates, λ is the wave length, and F is the focus length which can be chosen freely and arbitrarily. In our design, it is set as $F = 275$ mm to generate perfect vortex beams.

Thus, the total phase formula is expressed as follows:

$$\varphi_{tot}(x, y) = \varphi_1(x, y) + \varphi_2(x, y) \tag{5}$$

The spiral wavefront can be obtained by the metasurface with total phase distribution. In addition, vortex beams with narrow divergence angle can be generated theoretically.

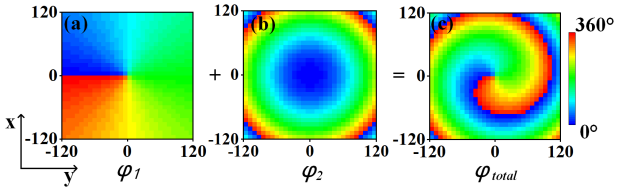

FIGURE 3. Calculating the phase distribution of the reflective metasurface. (a) vortex phase distribution, (b) focusing phase distribution, and (c) total phase distribution.

Figs. 3(a), (b), and (c) show the phase distribution of vortex, focusing and superimposing respectively.

According to the total phase distribution, the I-shaped unit cells are arranged to design a square aperture metasurface with the size of 240 mm×240 mm. The metasurface can generate vortex beams with narrow divergence angle, and will produce vortex wave of mode $l = 1$ under CP or LP waves incidence. The schematic model of the polarization insensitive metasurface is as shown in Fig. 4. In order to implement the proposed metasurface to generate vortex beams, a self-made axial mode helical antenna and rectangular waveguide antenna is adopted as LP and LCP feed source. The distance between the phase center of the feed antenna and metasurface aperture is 275 mm. Moreover, perfect vortex beams can be generated under LP or CP wave illumination without replacing the metasurface.

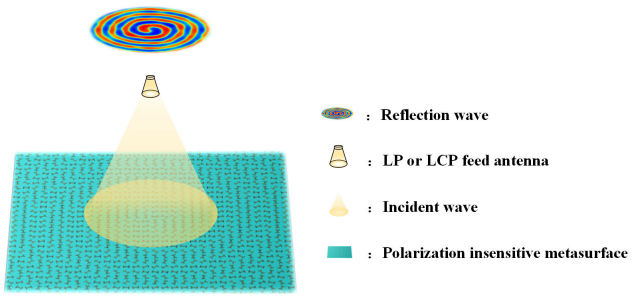

FIGURE 4. Schematic of the polarization insensitive metasurface for generating vortex waves.

IV. RESULTS AND DISCUSSION

A. SIMULATED RESULTS

To verify the effect of phase superposition method on reducing the beam divergence angle, the comparison between metasurface(M1) with only vortex phase distribution and metasurface(M2) with both vortex phase distribution and focusing phase distribution is performed under the incidence of LCP and LP waves. The corresponding 3D far-field patterns for LCP case at 16GHz are illustrated in Figs. 5(c) and (d), respectively. In Fig. 5(c), M1 generates vortex beams with scattered profile, which is hard to be received in practical application. This phenomenon is caused by the transverse vector of EM waves emitted by the feed antenna [32]. As for M2, a vortex beam with narrow divergence is obtained, as shown in Fig. 5(d). Intuitively, the divergence angle of the vortex beam is also reduced. The 3D far-field patterns of vortex beam reflected from

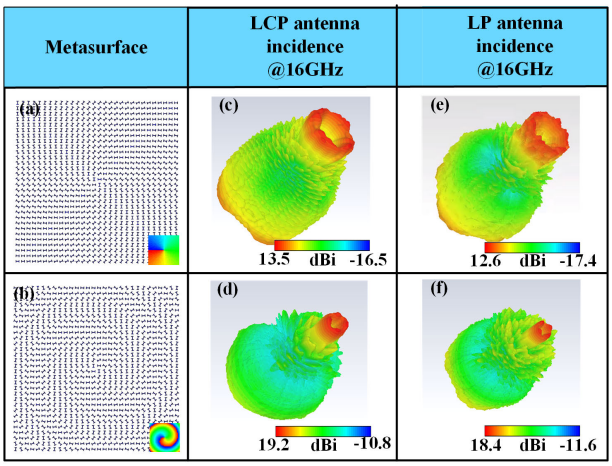

FIGURE 5. Proposed metasurfaces and their 3D far-field radiation patterns. (a) Metasurface (M1) with vortex phase distribution. (b) Metasurface (M2) with superposition phase distribution. (c), (d) 3D far-field radiation patterns of M1 and M2 under LCP waves incidence. (e), (f) 3D far-field radiation patterns of M1 and M2 under LP waves incidence.

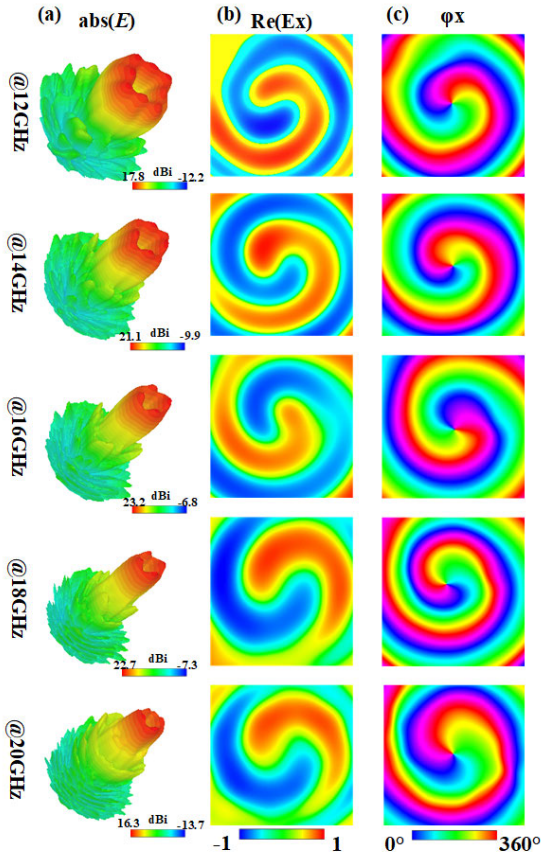

FIGURE 6. Numerical calculated far-field radiation patterns and E-field characteristics under normal excitation of LCP wave. (a) 3D far-field patterns at different frequencies. (b) Re(Ex) and (c) phase distributions from 12 GHz to 20 GHz in a step of 2 GHz.

M1 and M2 under LP wave incidence are presented in Figs. 5(e) and (f), respectively. In Fig. 5(f), a narrow vortex beam is obtained, and its divergence angle is smaller than that of the vortex beam in Fig. 5(e). These phenomena indicate that the focusing phase distribution effectively offsets the transverse vector to reduce divergence angle of vortex beams.

The far-field and near-field characteristics under LCP and LP waves incidence was presented, respectively. Fig. 6 shows the total 3D far-field radiation patterns and E-field characteristics at 12 GHz, 14 GHz, 16 GHz, 18 GHz, 20 GHz under LCP waves incidence. It is clear from Fig. 6(a) that the radiation energy is distributed around the beam and is extremely low in the normal direction, which is completely in line with the feature of an ideal vortex beam. The gain of vortex beams is better than 15 dBi within 10-20 GHz. Figs. 6 (b) and (c) show the simulation results of Re(Ex) and its phase distribution on the observed plane parallel to the metasurface under the excitation of the LCP feed antenna. All of the phase change once from 0° to 360°, which illustrated that the vortex beam carries OAM with $l = 1$.

In addition, a metasurface carrying the vortex phase distribution can generate similar LHCP and RHCP patterns under LP plane wave incidence, which are illustrated in Figs. 7 (a) and (b). This is quite physical because any LP wave with an arbitrary angle can be decomposed into an RHCP and an LHCP wave with equal magnitude. Figs. 7(c) and (d) clearly show that the magnitudes of RHCP and LHCP pattern from the proposed metasurface under normal incidence of LP feed antenna. The LHCP wave shows a doughnut-shaped intensity, which is consistent with the characteristics of vortex beam. The magnitude of RHCP component is so low that will not affect the OAM beam formation. In other words, the positive focusing phase is superimposed on the vortex metasurface, which compensates for the LHCP

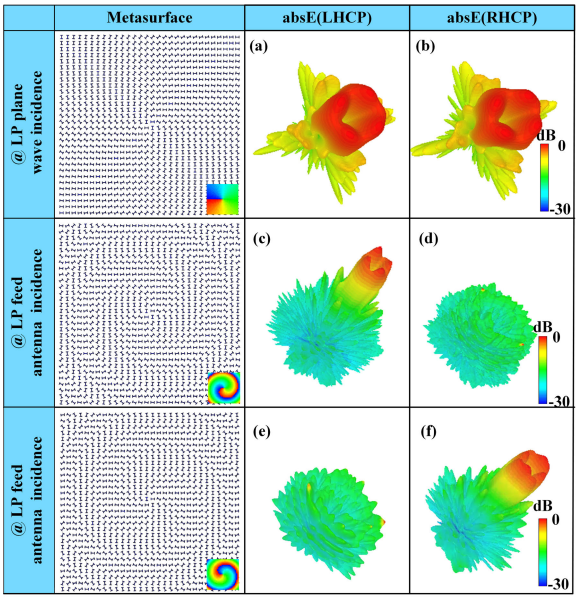

FIGURE 7. 3D far-field radiation patterns of metasurfaces with different phase distributions at 16GHz. (a) 3D radiation pattern of LHCP wave, and (b) RHCP wave generated by a metasurface with the vortex phase distribution under LP plane waves incidence. (c) 3D far-field pattern of LHCP wave, and (d) RHCP wave realized by a metasurface of phase distribution of $\phi_+ = \phi 1 + \phi 2$, and (e) 3D far-field pattern of LHCP wave, and (f) RHCP wave realized by a metasurface of phase distribution $\phi_- = \phi 1 - \phi 2$ under LP feed antenna excitation.

waves to generate ideal vortex beam and reduces the interference of the RHCP waves.

On the contrary, the metasurface generates a RHCP vortex beam and a very low radiation energy LHCP wave. The corresponding 3D radiation patterns are illustrated in Fig. 7(e) and (f).

As shown in Fig. 8, simulated results about far-field and near-field characteristics for LP case are listed to demonstrate the validity of proposed metesurface. Fig. 8(a) lists 3D radiation patterns of far-field at 12 GHz, 14 GHz, 16 GHz, 18 GHz, 20 GHz, which show the typical characteristics of the perfect vortex beam. The center of the beam is hollow, indicating that the radiation energy in the normal direction is extremely low. The Re(E_x) and phase distributions are similar to the LCP case, as shown in Figs. 8(b) and (c). The phase is consistent with the phase variation of the vortex beam with $l = 1$. These phenomena demonstrate the proposed metasurface can generate vortex beams with the OAM under LP waves incidence.

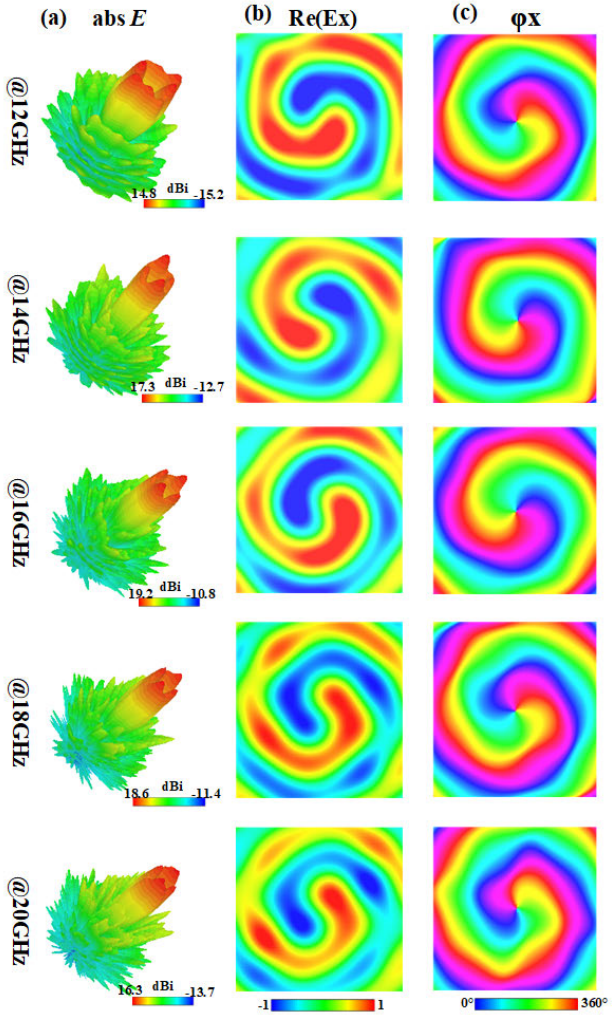

FIGURE 8. Simulated 3D far-field and near-field characteristics under normal incidence of LP wave. (a) 3D radiation patterns at different frequencies. (b) Re(Ex) and (c) phase distributions from 12 GHz to 20 GHz in a step of 2 GHz.

B. EXPERIMENTAL RESULTS

For experimental verification of the proposed design, a metasurface is fabricated using a printed circuit board (PCB) process. The size of the metasurface is 240 mm × 240 mm and consists of a 30 × 30 meta-atoms. Fig. 9 shows the experimental setup to measure the 2D far-field patterns in the microwave anechoic chamber. The feed antenna and sample of the proposed metasurface are shown in Figs. 9(b) and (c). The waveguide antenna is used as the linear polarization feed of the system. And the feed antenna is 275 mm apart from the proposed metasurface, which are fixed on the foam platform that can rotate around its central axis. The standard horn antenna is placed inside the red box in Fig. 9(d) and used as a receiving antenna to connect to the vector network analyzer to record the far-field information. The distance between the feed antenna and the receiving antenna is longer than 15 m. The center of the feed antenna, the receiving antenna and the metasurface are aligned to ensure the accuracy of measurement. Fig.9 (e) shows the schematic diagram of the experimental setup for better understanding how the resulting beam is measured.

The comparison between the experimental and simulated normalized 2D radiation pattern at 12 GHz, 14 GHz, 15 GHz, 16 GHz, 17 GHz, 18 GHz, which are shown in the Fig. 10. It can be clearly seen that a distinct amplitude null of vortex beams at $\theta = 0°$ from 12 GHz to 18 GHz. This phenomenon is consistent with the 3D far-field radiation patterns. This is complete to demonstrate that vortex beams are generated by the proposed metasurface under LP antenna incidence. The valley bottom is lower than −15 dB within 12-18 GHz, and the gain at normal direction is about −25.3 dB at 16 GHz.

Moreover, the divergence angles of vortex beams are 16°, 12°, 10°, 11°, 8°, 9° at 12 GHz, 14 GHz, 15 GHz, 16 GHz, 17 GHz, 18 GHz, respectively. The slight difference between

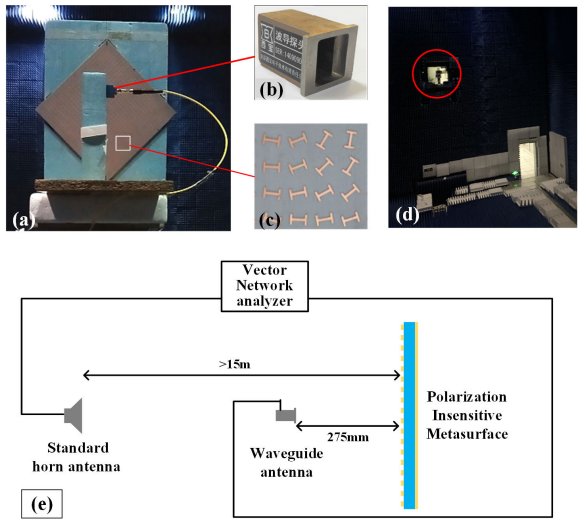

FIGURE 9. Experimental setup to measure the far fields of the fabricated metasurface. (a)The transmitting end. (b) The waveguide antenna as the feed source of the metasurface. (c) A zoom-in view of the sample. (d) The far view of the receiving end. (e) The schematic diagram of the experimental setup.

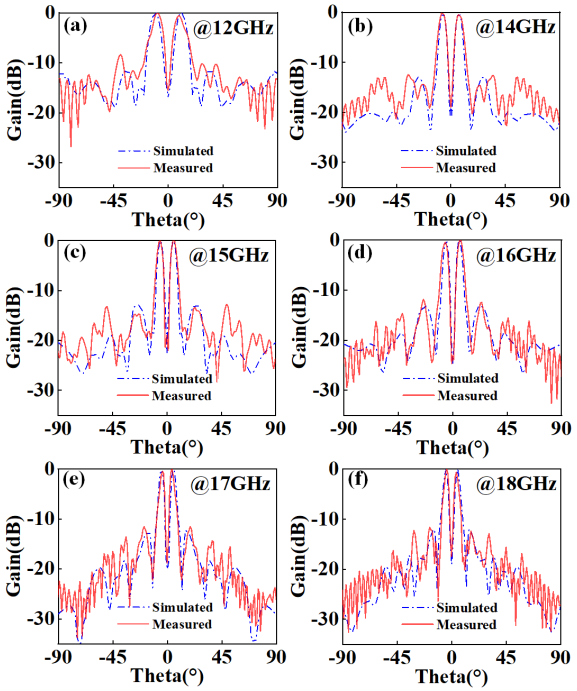

FIGURE 10. Comparison of simulated and measured 2D radiation patterns at xoz plane at the frequency range of 12-18 GHz.

simulated and measured curves is likely due to the measurement error and the deviation of the phase center.

V. CONCLUSION

In summary, we proposed a polarization insensitive metasurface using single-layer I-shaped elements to generate broadband vortex beam with narrow divergence angle. The phase superposition method is applied in the metasurface design to reduce the divergence angle of vortex beam. The proposed metasurface is composed of 30×30 reflective unit cells, which is not only suitable for LP wave excitation, but also for the CP wave incidence. The gain at normal direction is better than 15 dBi from 12 GHz to 20 GHz, and the maximum gain reaches 25.3 dBi and 23.2 dBi for LP and CP, respectively. A prototype is fabricated and tested, and the measured results are in good agreement with the simulation ones. The proposed design provides a flexible way to generate broadband and high gain vortex beams, which is important for increasing the wireless communication capacity.

REFERENCES

[1] S. Mohaghegh Mohammadi, L. K. S. Daldorff, J. E. S. Bergman, R. L. Karlsson, B. Thide, K. Forozesh, T. D. Carozzi, and B. Isham, "Orbital angular momentum in Radio—A system study," *IEEE Trans. Antennas Propag.*, vol. 58, no. 2, pp. 565–572, Feb. 2010.

[2] F. E. Mahmouli and S. D. Walker, "4-gbps uncompressed video transmission over a 60-GHz orbital angular momentum wireless channel," *IEEE Wireless Commun. Lett.*, vol. 2, no. 2, pp. 223–226, Apr. 2013.

[3] G. Gibson, J. Courtial, M. J. Padgett, M. Vasnetsov, and V. Pas'ko, "Free-space information transfer using light beams carrying orbital angular momentum," *Opt. Exp.*, vol. 12, no. 22, pp. 5448–5456, 2004.

[4] H. Chen, J. Hao, B.-F. Zhang, J. Xu, J. Ding, and H.-T. Wang, "Generation of vector beam with space-variant distribution of both polarization and phase," *Opt. Lett.*, vol. 36, no. 16, pp. 3179–3181, Aug. 2011.

[5] L. Allen, M. W. Beijersbergen, R. J. C. Spreeuw, and J. P. Woerdman, "Orbital angular momentum of light and the transformation of laguerre-Gaussian laser modes," *Phys. Rev. A, Gen. Phys.*, vol. 45, no. 11, pp. 8185–8189, Jun. 1992.

[6] Z. Zhang, S. Zheng, Y. Chen, X. Jin, H. Chi, and X. Zhang, "The capacity gain of orbital angular momentum based Multiple-Input-Multiple-Output system," *Sci. Rep.*, vol. 6, no. 1, pp. 1–11, Jul. 2016.

[7] Y. Yan, G. Xie, M. P. J. Lavery, H. Huang, N. Ahmed, C. Bao, Y. Ren, Y. Cao, L. Li, Z. Zhao, A. F. Molisch, M. Tur, M. J. Padgett, and A. E. Willner, "High-capacity millimetre-wave communications with orbital angular momentum multiplexing," *Nature Commun.*, vol. 5, no. 1, pp. 1–9, Dec. 2014.

[8] J. Wang, J.-Y. Yang, I. M. Fazal, N. Ahmed, Y. Yan, H. Huang, Y. Ren, Y. Yue, S. Dolinar, M. Tur, and A. E. Willner, "Terabit free-space data transmission employing orbital angular momentum multiplexing," *Nature Photon.*, vol. 6, no. 7, pp. 488–496, Jul. 2012.

[9] F. T. Mari and A. Sponselli, "Encoding many channels on the same frequency through radio vorticity: First experimental test," *New J. Phys.*, vol. 14, Mar. 2012, Art. no. 033001.

[10] M. Uchida and A. Tonomura, "Generation of electron beams carrying orbital angular momentum," *Nature*, vol. 464, no. 7289, pp. 737–739, Apr. 2010.

[11] P.-Y. Feng, S.-W. Qu, and S. Yang, "OAM-generating transmitarray antenna with circular phased array antenna feed," *IEEE Trans. Antennas Propag.*, vol. 68, no. 6, pp. 4540–4548, Jun. 2020.

[12] C. Deng, K. Zhang, and Z. Feng, "Generating and measuring tunable orbital angular momentum radio beams with digital control method," *IEEE Trans. Antennas Propag.*, vol. 65, no. 2, pp. 899–902, Feb. 2017.

[13] B. Thidé, H. Then, J. Sjöholm, K. Palmer, J. Bergman, T. D. Carozzi, Y. N. Istomin, N. H. Ibragimov, and R. Khamitova, "Utilization of photon orbital angular momentum in the low-frequency radio domain," *Phys. Rev. Lett.*, vol. 99, no. 8, p. 87701, Aug. 2007.

[14] S. Zheng, Y. Chen, Z. Zhang, X. Jin, H. Chi, X. Zhang, and Z. N. Chen, "Realization of beam steering based on plane spiral orbital angular momentum wave," *IEEE Trans. Antennas Propag.*, vol. 66, no. 3, pp. 1352–1358, Mar. 2018.

[15] N. Yu, P. Genevet, M. A. Kats, F. Aieta, J.-P. Tetienne, F. Capasso, and Z. Gaburro, "Light propagation with phase discontinuities: Generalized laws of reflection and refraction," *Science*, vol. 334, no. 6054, pp. 333–337, Oct. 2011.

[16] L. Zhang, S. Liu, L. Li, and T. J. Cui, "Spin-controlled multiple pencil beams and vortex beams with different polarizations generated by pancharatnam-berry coding metasurfaces," *ACS Appl. Mater. Interfaces*, vol. 9, no. 41, pp. 36447–36455, Oct. 2017.

[17] T. J. Cui, M. Q. Qi, X. Wan, J. Zhao, and Q. Cheng, "Coding metamaterials, digital metamaterials and programmable metamaterials," *Light: Sci. Appl.*, vol. 3, no. 10, p. e218, Oct. 2014.

[18] J. Yang, C. Zhang, H. F. Ma, J. Zhao, J. Y. Dai, W. Yuan, L. X. Yang, Q. Cheng, and T. J. Cui, "Generation of radio vortex beams with designable polarization using anisotropic frequency selective surface," *Appl. Phys. Lett.*, vol. 112, no. 20, May 2018, Art. no. 203501.

[19] S. Yu, L. Li, G. Shi, C. Zhu, and Y. Shi, "Generating multiple orbital angular momentum vortex beams using a metasurface in radio frequency domain," *Appl. Phys. Lett.*, vol. 108, no. 24, Jun. 2016, Art. no. 241901.

[20] L. Yu, X. Li, Z. Qi, H. Zhu, Y. Huang, and Z. Akram, "Wideband circularly polarized dual-mode vortex beams reflectarray design using Dual-Semi-Split-Loop elements," *IEEE Antennas Wireless Propag. Lett.*, vol. 18, no. 12, pp. 2676–2680, Dec. 2019.

[21] C. Ji, J. Song, C. Huang, X. Wu, and X. Luo, "Dual-band vortex beam generation with different OAM modes using single-layer metasurface," *Opt. Exp.*, vol. 27, no. 1, pp. 34–44, Jan. 2019.

[22] S. Tang, X. Li, W. Pan, J. Zhou, T. Jiang, and F. Ding, "High-efficiency broadband vortex beam generator based on transmissive metasurface," *Opt. Exp.*, vol. 27, no. 4, pp. 4281–4291, 2019.

[23] K. Zhang, "Phase-engineered metalenses to generate converging and non-diffractive vortex beam carrying orbital angular momentum in microwave region," *Opt. Exp.*, vol. 26, no. 2, pp. 1351–1360, Jan. 2018.

[24] W.-L. Guo, G.-M. Wang, K. Chen, H.-P. Li, Y.-Q. Zhuang, H.-X. Xu, and Y. Feng, "Broadband polarization-conversion metasurface for a cassegrain antenna with high polarization purity," *Phys. Rev. A, Gen. Phys.*, vol. 12, no. 1, Jul. 2019, Art. no. 014009.

[25] W. Luo, S. Sun, H.-X. Xu, Q. He, and L. Zhou, "Transmissive ultrathin pancharatnam-berry metasurfaces with nearly 100% efficiency," *Phys. Rev. A, Gen. Phys.*, vol. 7, no. 4, Apr. 2017, Art. no. 044033.

[26] S. Yu, L. Li, G. Shi, C. Zhu, X. Zhou, and Y. Shi, "Design, fabrication, and measurement of reflective metasurface for orbital angular momentum vortex wave in radio frequency domain," *Appl. Phys. Lett.*, vol. 108, no. 12, Mar. 2016, Art. no. 121903.
[27] G.-T. Chen, Y.-C. Jiao, and G. Zhao, "A reflectarray for generating wide-band circularly polarized orbital angular momentum vortex wave," *IEEE Antennas Wireless Propag. Lett.*, vol. 18, no. 1, pp. 182–186, Jan. 2019.
[28] Z. Akram, X. Li, Z. Qi, A. Aziz, L. Yu, H. Zhu, X. Jiang, and X. Li, "Wide-band vortex beam reflectarray design using quarter-wavelength element," *IEEE Antennas Wireless Propag. Lett.*, vol. 18, no. 7, pp. 1458–1462, Jul. 2019.
[29] J. Yang, "Tailoring polarization states of multiple beams that carry different topological charges of orbital angular momentums," *Opt. Exp.*, vol. 26, no. 24, pp. 31664–31674, 2018.
[30] L. Yu, X. Li, Z. Qi, H. Zhu, Y. Huang, and Z. Akram, "Wideband circularly polarized high-order bessel beam reflectarray design using Multiple-Ring-Cascade elements," *IEEE Antennas Wireless Propag. Lett.*, vol. 19, no. 7, pp. 1226–1230, Jul. 2020.
[31] L.-J. Yang, S. Sun, and W. E. I. Sha, "Ultrawideband reflection-type metasurface for generating integer and fractional orbital angular momentum," *IEEE Trans. Antennas Propag.*, vol. 68, no. 3, pp. 2166–2175, Mar. 2020.
[32] H. Wang, Y. Li, Y. Han, Y. Fan, S. Sui, H. Chen, J. Wang, Q. Cheng, T. Cui, and S. Qu, "Vortex beam generated by circular-polarized metasurface reflector antenna," *J. Phys. D, Appl. Phys.*, vol. 52, no. 25, Jun. 2019, Art. no. 255306.
[33] Y. Ran, J. Liang, T. Cai, and H. Li, "High-performance broadband vortex beam generator using reflective Pancharatnam–Berry metasurface," *Opt. Commun.*, vol. 427, pp. 101–106, Nov. 2018.
[34] H. Xu, H. Liu, X. Ling, Y. Sun, and F. Yuan, "Broadband vortex beam generation using multimode Pancharatnam–Berry metasurface," *IEEE Trans. Antennas Propag.*, vol. 65, no. 12, pp. 7378–7382, Dec. 2017.

HONGYU MA received the M.S. degree from the Harbin Institute of Technology, Harbin, China, in 2001, and the Ph.D. degree in electronics engineering from the Key Laboratory of MEMS of the Ministry of Education, Southeast University, Nanjing, China, in 2010, respectively. After graduation, he joined the Research Center for the Internet of Things, China University of Mining and Technology. He was a Visiting Researcher with the Berkeley Sensor and Actuator Center, Department of Mechanical Engineering, University of California, Berkeley, CA, USA, from February 2016 to January 2017. He is currently an Associate Professor and also working towards the micro-methane sensor for IoT in coalmine and other filed. His research interests include integrated sensors, as well as micromachining and fabrication for microsensors.

XIANGLIN KONG (Member, IEEE) was born in Shandong, China. He received the B.S. degree from Dezhou University, Dezhou, China, in 2017. He is currently pursuing the M.S. degree with the China University of Mining and Technology, Xuzhou, China. His research interests include the design of RF/microwaves antennas and metasurface.

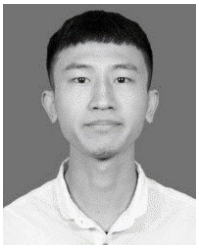

PENG CHEN (Member, IEEE) was born in Hebei, China. He received the B.S. degree from the Tianjin University of Technology, Tianjin, China, in 2017. He is currently pursuing the M.S. degree with the China University of Mining and Technology, Xuzhou, China. His research interest includes the design of RF/microwaves absorber.

WEIHUA WANG was born in Jiangsu, China. He received the Ph.D. degree in physics from Fudan University, Shanghai, China, in 2010. From September 2010 to January 2013, he was a Postdoctoral Fellow of the Chalmers Institute of Technology, Sweden. From April 2013 to March 2015, he was a Postdoctoral Fellow of the Technical University of Denmark. He joined the School of Physical Science and Technology, China University of Mining and Technology, Xuzhou, China, in 2018. He is as a Reviewer of multiple journals, including the *Physical Review A*, *Physical Review B*, *Physical Review Letters*, and *Optics Express*.

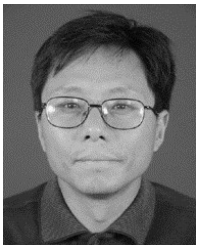

KUI HAN received the B.S. degree in physical education from Jiangsu Normal University, China, in 1985, and the M.S. and Ph.D. degrees in physics from Fudan Universitu, Shanghai, China, in 1995 and 1998, respectively. In June 2000, he joined the School of Physical Science and Technology, China University of Mining and Technology, Xuzhou, China. From August 1985 to July 1992, he worked with Jiangsu Normal University, Xuzhou.

LEI ZHAO (Senior Member, IEEE) received the B.S. degree in mathematics from Jiangsu Normal University, China, in 1997, and the M.S. degree in computational mathematics and the Ph.D. degree in electromagnetic fields and microwave technology from Southeast University, Nanjing, China, in 2004 and 2007, respectively.

He joined the China University of Mining and Technology, Xuzhou, China, in 2019, where he is currently a Full Professor. From September 2009 to December 2018, he worked with Jiangsu Normal University, Xuzhou, China. From August 2007 to August 2009, he worked with the Department of Electronic Engineering, The Chinese University of Hong Kong, as a Research Associate. From February 2011 to April 2011, he worked with the Department of Electrical and Computer Engineering, National University of Singapore, as a Research Fellow. From September 2016 to September 2017, he worked with the Department of Electrical and Computer Engineering, University of Illinois at Urbana–Champaign, Champaign, IL, USA, as a Visiting Scholar. He has authored or coauthored more than 60 refereed journal and conference papers. His current research interests include spoof surface plasmon polaritons theory and its applications, RF/microwave antenna and filter design, computational electromagnetics, and electromagnetic radiation to human's body.

Dr. Zhao serves as an Associate Editor for IEEE Access, the Associate Editor-in-Chief for the *ACES Journal*, and a Reviewer for multiple journals and conferences, including the IEEE Transactions on Microwave Theory and Techniques, the IEEE Transactions on Antennas and Propagation, IEEE Access, the IEEE Antennas and Wireless Propagation Letters, *ACES Journal*, and other primary electromagnetics and microwave related journals.

XIAOPENG SHEN (Member, IEEE) received the B.S. degree in physical education from Qufu Normal University, in 1997, and the second B.S. degree in internal trade and the M.S. degree in theory physics from the China University of Mining and Technology, Xuzhou, China, in 1997 and 2006, respectively. In August 1999, he joined the School of Physical Science and Technology, China University of Mining and Technology, as a Lecturer, and became an Associate Professor, in 2008. His current research interests include photonic crystals, plasmonics, and metamaterials. He received the Second Prize of the National Natural Science Award of China in 2018.